



**HAL**  
open science

## Elucidating the nature of the external acid sites of ZSM-5 zeolites using NMR probe molecules

Carlos Bornes, Dusan Stosic, Carlos Geraldès, Svetlana Mintova, João Rocha,  
Luís Mafra

► **To cite this version:**

Carlos Bornes, Dusan Stosic, Carlos Geraldès, Svetlana Mintova, João Rocha, et al.. Elucidating the nature of the external acid sites of ZSM-5 zeolites using NMR probe molecules. *Chemistry - A European Journal*, 2022, 28 (64), 10.1002/chem.202201795 . hal-04295937

**HAL Id: hal-04295937**

**<https://hal.science/hal-04295937v1>**

Submitted on 20 Nov 2023

**HAL** is a multi-disciplinary open access archive for the deposit and dissemination of scientific research documents, whether they are published or not. The documents may come from teaching and research institutions in France or abroad, or from public or private research centers.

L'archive ouverte pluridisciplinaire **HAL**, est destinée au dépôt et à la diffusion de documents scientifiques de niveau recherche, publiés ou non, émanant des établissements d'enseignement et de recherche français ou étrangers, des laboratoires publics ou privés.

# Elucidating the nature of the external acid sites of ZSM-5 zeolites using NMR probe molecules

Carlos Bornes,<sup>[a]</sup> Dusan Stosic,<sup>[b]</sup> Carlos F. G. C. Geraldès,<sup>[c,d]</sup> Svetlana Mintova,<sup>\*[b]</sup> João Rocha,<sup>\*[a]</sup> Luís Mafrá<sup>\*[a]</sup>

[a] C. Bornes, Prof. Dr. J. Rocha, Dr. L. Mafrá  
CICECO, Aveiro Institute of Materials, Department of Chemistry  
University of Aveiro  
3810-193 Aveiro, Portugal  
E-mail: [rocha@ua.pt](mailto:rocha@ua.pt), [lmafra@ua.pt](mailto:lmafra@ua.pt)

[b] Dr. D. Stosic, Prof. Dr. S. Mintova  
Laboratoire Catalyse & Spectrochimie (LCS)  
Normandie Univ  
ENSICAEN, UNICAEN, CNRS, 14000 Caen, France  
E-mail: [svetlana.mintova@ensicaen.fr](mailto:svetlana.mintova@ensicaen.fr)

[c] Prof. Dr. C. F. G. C. Geraldès  
Department of Life Sciences and Coimbra Chemistry Center, Faculty of Science and Technology  
University of Coimbra  
3000-393 Coimbra, Portugal

[d] CIBIT-Coimbra Institute for Biomedical Imaging and Translational Research  
3000-548 Coimbra, Portugal

**Abstract:** The identification of acid and nonacid species at the external surface of zeolites remains a major challenge, in contrast with the much-studied internal acid sites. Here, we show that the synthesis of zeolite ZSM-5 samples with distinct particle sizes, combined with solid-state NMR and computational studies of trimethylphosphine oxide (TMPO) adsorption, provides insight into the chemical species on the external surface of the zeolite crystals.  $^1\text{H}$ - $^{31}\text{P}$  HETCOR NMR spectra of TMPO-loaded zeolites exhibit a broad correlation peak at  $\delta_{\text{P}} \sim 35 - 55$  ppm and  $\delta_{\text{H}} \sim 5 - 12$  ppm assigned to external SiOH species. Pore-mouth Brønsted acid sites exhibit  $^{31}\text{P}$  and  $^1\text{H}$  NMR resonances and adsorption energies close to those reported for internal acid sites interacting with TMPO. The presence of an external tricoordinate Al-Lewis site interacting strongly with TMPO is suggested, resulting in  $^{31}\text{P}$  resonances that overlap with the peaks usually ascribed to the interaction of TMPO with Brønsted sites.

## Introduction

Zeolites are crystalline hydrated microporous aluminosilicate materials constructed from corner sharing  $\text{SiO}_4$  and  $\text{AlO}_4$  tetrahedra, and commercially employed in catalysis,<sup>[1]</sup> adsorption (separation),<sup>[2]</sup> and ion-exchange applications.<sup>[3]</sup> Because of their unique microporous structure endowing them with size and shape selective catalytic properties, zeolites account for over 40% of the solid catalysts used in the chemical industry.<sup>[4]</sup> Many recent studies show that the reduction of zeolites' particle size from the micrometer to nanometer range improves the catalytic activity,<sup>[5-7]</sup> and reduces coke formation.<sup>[6]</sup> Reports on the improved catalytic activity of these ultrafine catalysts are available for a variety of reactions including fluid catalytic cracking,<sup>[8]</sup> methanol to propylene,<sup>[5-7]</sup> hydroxylation of phenol,<sup>[9]</sup> isomerization of xylene,<sup>[10]</sup> and amination of methanol.<sup>[11]</sup> The improvement of the catalytic activity is usually ascribed to the shortening of the diffusion paths within zeolite channels that increase the mass transport, external surface area, number of pore-mouth active sites, and the accessibility of molecules to the acid sites.

Acidity is another crucial factor determining the catalytic activity of zeolites, such as ZSM-5. Notwithstanding, the acid properties of nanosized zeolites are still poorly understood, in contrast with their micron-scale counterparts. Zhang et al., studied H-ZSM-5 zeolites with particle sizes in the range 1000 nm to 70 nm by solid-state NMR, observing an increase in the concentration of SiOH groups and Brønsted acid sites at the crystals' external surface with decreasing particle size.<sup>[12]</sup> They concluded that decreasing the particle size increases the local structure disorder. Louis et al., reported similar findings concerning the SiOH groups but found no significant differences in the total number of acid sites.<sup>[13]</sup> Gehring et al., investigated nanosized and micronsized H-ZSM-5 zeolites with Si/Al atomic ratios of 31–88.<sup>[14]</sup> The results indicated that while the aluminium atoms are in tetrahedrally-coordinated framework positions in the nanosized materials only 32% - 34% of these atoms contribute to the formation of Brønsted acid sites arising from bridging OH groups (Si(OH)Al). The remaining framework aluminium species lead to the formation of silanol groups with weakly enhanced Brønsted acidity (Si(OH)···Al), comparable to amorphous aluminosilicates. On the other hand, Treps et al., have recently investigated the surface speciation of silicalite-1 and ZSM-5 crystals by computational methods that excluded the formation of pseudo-bridging hydroxyl groups (Si(OH)···Al). Instead, AlOH, pore-mouth bridging hydroxyl groups, and Al-H<sub>2</sub>O, were suggested as possible external surface species.<sup>[15]</sup> The latter can undergo dehydration, exposing the Al atom and creating a Lewis acid site.

$^{31}\text{P}$ -bearing probe molecules, mainly trimethylphosphine oxide (TMPO), have been widely used to study the acid properties of several acidic materials, such as zeolites. Contrary to other larger-sized alkylphosphine oxides, TMPO can diffuse through most mid to large-pore zeolites. TMPO interacts with both Brønsted and Lewis acid sites giving rise to  $^{31}\text{P}$  resonances between 53 and 86 ppm and between 55 and 60 ppm, respectively. However, the origin of  $^{31}\text{P}$  resonances below 60 ppm is still controversial.

Here, we provide new atomic-level insight into the nature of the external surface sites of ZSM-5. Zeolites with distinct particle size and acid properties were studied via the interaction of

TMPO molecules with the internal and external sites using solid-state NMR and computational methods.

## Results and Discussion

Powder XRD indicates that the nanosized and micronized zeolite samples exhibit high crystallinity and the MFI-type framework structure (Figure S1). DLS reveals a monomodal particle size distribution for both zeolites, and mean crystals' hydrodynamic diameters of 180 nm and 980 nm for nanosized and micronized samples, respectively (Figure S2). The crystals' morphology was ascertained by SEM (Figure 1). Micronized ZSM-5 exhibits crystals with the typical coffin-like shape and some rounded-boat crystals. The nanosized sample consists mostly of rounded-boat crystals. These are the two most common morphologies of MFI-type crystals, and it has been observed that in the crystallization process the smaller rounded-boat crystals evolve into larger coffin-shaped crystals.[16,17]

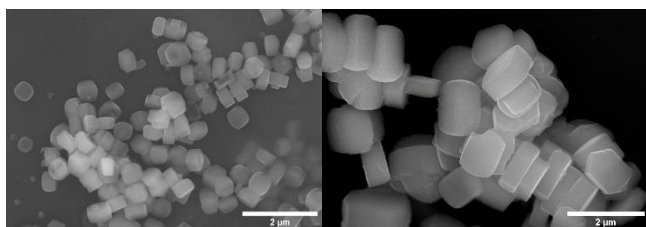


**Figure 1.** SEM micrographs of nanosized (left) and micronized (right) ZSM-5 zeolite samples.

Nitrogen adsorption measurements were performed to characterize the porosity of the materials (Figure S3). Micronized ZSM-5 exhibits the classical Type I isotherm, with a sharp uptake at low relative pressures, followed by horizontal adsorption and desorption branches. Nanosized ZSM-5, in turn, exhibits a mix of Type I and IV isotherms with a large H1-type hysteresis. The latter feature is ascribed to the formation of textural pores by the close packing of monodispersed and well-shaped nanosized zeolite crystals. The micropore volume of nano- and micronized zeolites is  $0.16 \text{ cm}^3 \cdot \text{g}^{-1}$ , witnessing the high crystallinity of the samples. The nanosized zeolite has the additional mesopore volume of  $0.12 \text{ cm}^3 \cdot \text{g}^{-1}$ . These results are in a good accord with the literature.[18]

Consider Figure 2a, b. Prior to H-exchange, the  $^{31}\text{P}$  MAS NMR spectra of TMPO-loaded calcined nanosized and micronized ZSM-5 exhibit mainly resonances below  $\sim 60$  ppm. The weak peaks above 60 ppm indicate that burning the organic structure-directing agent leaves behind some protons acting as Brønsted acid sites (see below). The TMPO loading used ensures the full coverage of the bare Brønsted acids sites, witnessed by the absence of a  $^1\text{H}$  MAS NMR resonance at 4.3 ppm (Figure S4).[19] Spectra deconvolution shows that the intensity of  $^{31}\text{P}$  NMR resonances above 60 ppm accounts for 2.8% and 12.0% of the TMPO-interacting species for the calcined nanosized and micronized ZSM-5 samples, respectively (Table S1). As expected, the H-exchange step considerably increases the number of Brønsted acid sites present: the intensity of  $^{31}\text{P}$  NMR resonances above 60 ppm accounts for 37.0% and 40.8% for the nanosized- and micronized H-exchanged ZSM-5 samples, respectively. Since the micronized zeolites have a higher

internal-to-external surface area ratio when compared to their nanosized counterparts, we hypothesize that the higher relative intensity of  $^{31}\text{P}$  NMR resonances above 60 ppm arises from a larger number of TMPO molecules interacting with the internal surface acid sites. Note that this is observed for both the calcined and H-exchanged zeolites.

In a previous work, we have shown that  $^{31}\text{P}$  NMR resonances at ca. 64 ppm, 69 ppm and 76 ppm are ascribed to protonated TMPO molecules sitting at the different channels and channel intersections of H-ZSM-5.[20] In contrast, the nature of the TMPO-interacting species giving the  $^{31}\text{P}$  NMR resonances below 60 ppm is contentious. They have been assigned to the interaction of TMPO with terminal silanol groups,[21] formation of  $(\text{TMPO})_2\text{H}^+$  dimers,[20,22] interaction with Lewis acid sites,[23] weak Brønsted acid sites,[24] and physisorbed ( $\sim 44$  ppm), crystalline ( $\sim 41$  ppm), confined ( $\sim 37$  ppm), and mobile TMPO ( $\sim 31$  ppm). These conflicting assignments do not elucidate the reason for the higher relative spectral intensity below 60 ppm for the micronized zeolite sample, as compared with the nanosized sample.

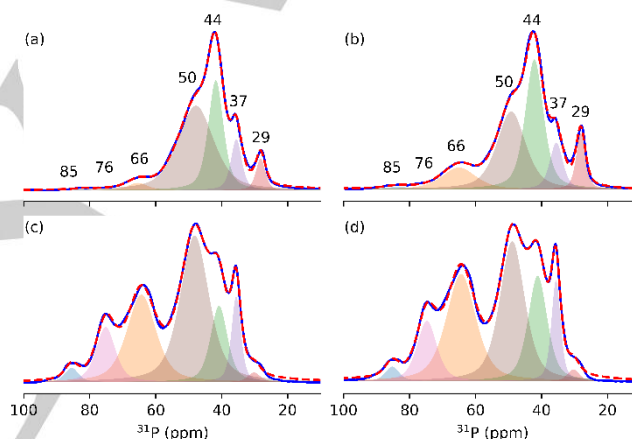


**Figure 2.**  $^{31}\text{P}$  MAS NMR spectra of TMPO-loaded calcined (a) nanosized and (b) micronized ZSM-5, and H-exchanged (c) nanosized and (d) micronized ZSM-5 zeolites.

Figure 3 shows the  $^1\text{H}$ - $^{31}\text{P}$  HETCOR NMR spectra of TMPO-loaded calcined and H-exchanged nanosized and micronized ZSM-5. The correlation peak at  $\delta_{\text{H}} \sim 1$  to 2 ppm, spanning 60 ppm in the  $^{31}\text{P}$  dimension, is assigned to the autocorrelation between TMPO phosphorous and the methyl protons.  $^1\text{H}$ - $^{31}\text{P}$  HETCOR NMR spectra of the H-exchanged samples (Figure 3c and d) exhibit the typical U-shaped correlation peak ranging from 12 to 16 ppm.[20,22] In contrast, this spectral feature is much weaker for calcined ZSM-5 samples (Figure 3a, b). Such broad correlation peaks have been assigned to protonated TMPO molecules sitting at the straight channels, sinusoidal channels, and channel intersections, for (resonances above 60 ppm), and to  $(\text{TMPO})_2\text{H}^+$  dimers (resonances below 60 ppm).[20] The low intensity of the correlation peaks observed for the calcined samples is ascribed to the small number of Brønsted acid sites left after burning the organic structure directing agent ( $\text{TPA}^+$ ). The  $^{29}\text{Si}$  MAS NMR spectra of the calcined nanosized and micronized samples (Figure S5) are dominated by the Q4(OAl) resonance at ca. -112 (with a shoulder at -115 ppm) showing also a small peak at ca. -104 ppm that comprises Q<sup>4</sup>(1Al), Q<sup>3</sup>(OAl), and Q<sup>2</sup>(OAl) species.[25]

Upon  $^1\text{H}$ - $^{29}\text{Si}$  cross-polarization, the spectrum is dominated by a peak at -102 ascribed to Q3(OAl) and, as expected, the intensity of the Q4(OAl) peak at -112 ppm is much reduced. The faint resonance at -94 ppm is assigned to Q2(OAl) species. These observations have been widely reported in the literature, according to which SiOH groups are formed by reaction of defect  $\text{SiO}^-$  sites with the protons resulting from the  $\text{TPA}^+$  decomposition.[25]

All samples also exhibit a broad  $^{31}\text{P}$  correlation peak in the range  $\sim 35 - 55$  ppm and  $^1\text{H}$  resonances in the range  $\sim 5 - 12$  ppm. Similar correlation peaks have been assigned to the interaction of TMPO with trace amounts of template molecules,[22] and to TMPO physisorption.[26] The  $35 - 55$  ppm  $^{31}\text{P}$  NMR spectral intensity increases relatively to the  $55 - 100$  ppm intensity with decreasing particle size, the respective ratios (calculated from deconvolution of the  $^{31}\text{P}$  MAS NMR spectra in Figure 2, see Table S1) are: 33.3% and 6.7% for the calcined nanosized and micronsized samples, respectively; and 1.7% and 1.4% for the H-exchanged nanosized and micronsized samples, respectively. In addition, the calculated volume of the  $^1\text{H}$ - $^{31}\text{P}$  HETCOR NMR correlation peaks at  $\delta_{\text{P}} \sim 35 - 55$  ppm and  $\delta_{\text{H}} \sim 5 - 12$  ppm for the nanosized samples is twice their micronsized counterparts for both the calcined and the H-exchanged samples. This suggests that the correlation peak at  $\delta_{\text{P}} \sim 35 - 55$  ppm and  $\delta_{\text{H}} \sim 5 - 12$  ppm arises from the interaction of TMPO with external species, as its intensity is higher for the nanosized samples. Adsorbing TMPO on nanosized silicalite-1 crystals, the pure Si analogue of ZSM-5 with particle size 250 - 800 nm (Figure S6), leads to a similar correlation peak (Figure S7). The absence of Al in silicalite-1 and, thus, of Brønsted and Lewis acid sites, confirms that this correlation peak is due to the interaction of TMPO with Si-species, such as SiOH, as suggested in a recent study.[21]

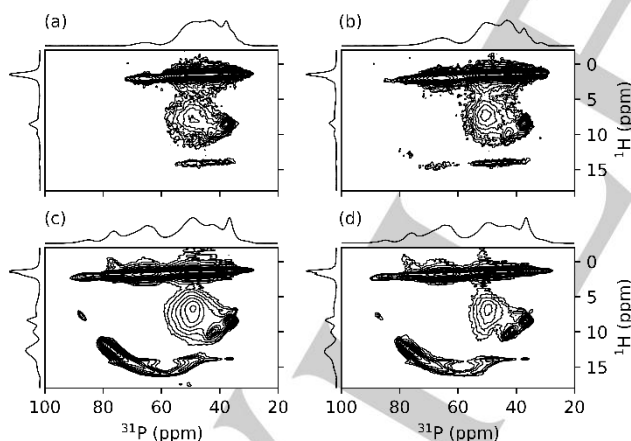


**Figure 3.**  $^1\text{H}$ - $^{31}\text{P}$  HETCOR NMR spectra of TMPO-loaded calcined (a) nanosized and (b) micronsized ZSM-5 samples; H-exchanged (c) nanosized and (d) micronsized ZSM-5 zeolite samples.

Because all samples described in this work contain particles of smaller size than the samples studied in previous NMR studies, and no treatment was performed to change the external surface of the materials, the correlation peak at  $\delta_{\text{H}} \sim 5$  to 12 ppm is assigned to TMPO interaction with sites at the external surface of the crystals. Although it is often assumed that the external surface of zeolite crystals is coated with SiOH groups, other

external surface species have been proposed for silicalite-1 and ZSM-5.[15]

To get further insight into the nature of the species associated with the NMR cross peaks, the interaction of TMPO with distinct external surface species and ensuing  $^1\text{H}$  and  $^{31}\text{P}$  NMR chemical shifts were studied by adapting the models of Chizallet group.[15] We have modeled the interaction of TMPO with terminal SiOH groups, pore-mouth bridging hydroxyl groups (SiOHAl), water coordinated Al- $\text{H}_2\text{O}$  species, Al-Lewis acid centers, and internal SiOH nests (Figure 4). Next, we present the results of these studies.

#### TMPO – pore-mouth SiOHAl surface interactions

The adsorption energies of TMPO with pore-mouth SiOHAl groups (Figure 4a) are in the range  $-151 \text{ kJ}\cdot\text{mol}^{-1}$  to  $-184 \text{ kJ}\cdot\text{mol}^{-1}$  (Table S2). These values are in between  $-236 \text{ kJ}\cdot\text{mol}^{-1}$  and  $-142 \text{ kJ}\cdot\text{mol}^{-1}$ , the values previously reported for TMPO interacting with Brønsted acid sites at H-ZSM-5 channel intersection and channels, respectively.[20] The interaction with pore-mouth Brønsted acid sites results in the protonation of TMPO, yielding  $^{31}\text{P}$  NMR resonances in the range 66 ppm - 69 ppm (Table S2), similar to those of internal acid sites.[20] This indicates that the strength of the pore-mouth and internal acid sites is similar, illuminating the nature of the species involved in pore-mouth catalysis.[27,28]

#### TMPO – SiOH surface interactions

The interaction of TMPO with a single SiOH (SiOH-iso) and with two vicinal SiOH (SiOH-vic) groups was considered. The interaction with the external SiOH groups results in hydrogen-bonded TMPO and higher adsorption energies,  $-121 \text{ kJ}\cdot\text{mol}^{-1}$  (SiOH-iso) and  $-132 \text{ kJ}\cdot\text{mol}^{-1}$  (SiOH-vic) (Table S3), when compared with internal and external bridging hydroxyl groups, witnessing the weak SiOH acid strength. The interaction with the SiOH-iso group (Figure 4c) yields calculated  $^{31}\text{P}$  and  $^1\text{H}$  NMR chemical shifts of 32.5 ppm and 9.4 ppm, respectively. In turn, the interaction with the SiOH-vic groups (Figure 4b) affords  $^{31}\text{P}$  and  $^1\text{H}$  NMR chemical shifts of 43.4 ppm and 7.4 ppm (Table S3) that fall in the broad correlation peak at  $\delta_{\text{P}} = 55 - 35$  ppm and  $\delta_{\text{H}} = 7 - 12$  ppm. The width of this peak is ascribed to the large number of possible TMPO sitting sites at the distinct ZSM-5 crystallographic facets with different local chemical environments and, hence, slightly different  $^{31}\text{P}$  and  $^1\text{H}$  NMR chemical shifts. The formation of other silanol species, such as geminal, bridged silanols, and  $[\text{SiO}^-\cdots\text{HOSi}]$  clusters, proposed as possible crystal termination species,[29] may also contribute to the broadening of this correlation peak. The interaction of TMPO with internal silanol nests (Figure 4d) was also studied to assess the effect of the pore confinement on the TMPO...SiOH interaction. The calculations yielded a  $^{31}\text{P}$  NMR resonance in the range of external SiOH sites,  $\delta_{\text{P}} = 43.5$  ppm, and a  $^1\text{H}$  NMR resonance at  $\delta_{\text{H}} = 15.5$  ppm (Table S3). A similar correlation peak appears for all samples studied (Figure 3), including silicalite-1 (Figure S7), thus suggesting the presence of internal SiOH groups.

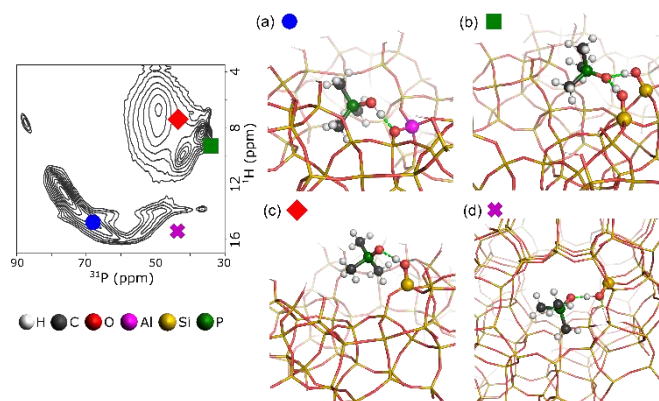


**Figure 4.** Models of TMPO interacting with: (a) pore-mouth bridging hydroxyl groups, (b) two vicinal SiOH groups, (c) one isolated SiOH group, and (d) internal silanol nest (on the right). The respective calculated  $^{31}\text{P}$  and  $^1\text{H}$  NMR chemical shifts are depicted on the  $^1\text{H}$ - $^{31}\text{P}$  HETCOR NMR spectrum of nanosized H-ZSM-5 (left).

### TMPO – Al surface interactions

The calculated adsorption energies of TMPO on the external Al-H<sub>2</sub>O species are  $-187\text{ kJ}\cdot\text{mol}^{-1}$  and  $-165\text{ kJ}\cdot\text{mol}^{-1}$  (Table S4), in line with the values obtained for the pore-mouth sites. However, because TMPO adsorption is performed on fully dehydrated zeolites these species tend to undergo dehydration and form three-coordinated Al-species that act as Lewis acid sites.<sup>[15]</sup> Adding a TMPO molecule to these Al-Lewis sites results in tetra-coordinated Al-species (Figure S8) appearing at 63.2 ppm - 60.3 ppm in the  $^{31}\text{P}$  NMR spectrum (Table S5). Unfortunately, this resonance falls in the same region of TMPO molecules interacting with Brønsted acid sites at the pore-mouth and at the straight channels; and the lack of a H-mediated interaction results in no correlation peak, hindering the spectral identification of these species. TMPO interacts strongly with these Al-Lewis sites, with adsorption energies  $-247\text{ kJ}\cdot\text{mol}^{-1}$  and  $-253\text{ kJ}\cdot\text{mol}^{-1}$ . The stronger interaction with these sites relatively to SiOH and Brønsted acid sites suggests that Al-Lewis sites are populated first upon TMPO adsorption. This observation supports the appearance of  $^{31}\text{P}$  NMR resonances at  $\sim 60$  ppm with no correlation with  $^1\text{H}$  resonances that have been previously reported for very low TMPO-loadings.<sup>[26]</sup>

### Conclusion

Though the internal zeolite acid sites have been much studied using probe molecules, establishing the nature of their external surface acid and nonacid species remains a major challenge. The study of TMPO adsorption on ZSM-5 samples with distinct particle sizes and acid properties by solid-state NMR and computational methods sheds new light on the chemical species present on the crystals external surface.  $^1\text{H}$ - $^{31}\text{P}$  HETCOR NMR spectra of TMPO-loaded zeolites with small particle size exhibit a broad correlation peak at  $\delta_{\text{P}} \sim 35 - 55$  ppm and  $\delta_{\text{H}} \sim 5 - 12$  ppm assigned to the external SiOH species. The intensity of this correlation peak is larger for nanosized zeolites, as compared with the micronized sample, supporting its assignment to external surface sites. Because this correlation peak is observed prior to the H-exchange step, and in a pure-Si MFI sample, it is assigned to SiOH species. The pore-mouth Brønsted acid sites exhibit  $^{31}\text{P}$  and  $^1\text{H}$  NMR chemical shifts close to those previously reported for the interaction of TMPO molecules with straight and sinusoidal channels. The interaction with pore-mouth acid sites

results in TMPO protonation and adsorption energies like the interaction with internal acid sites. The interaction with external tricoordinate Al-Lewis sites stemming from the dehydration of Al-H<sub>2</sub>O species yields  $^{31}\text{P}$  NMR resonances at  $\sim 60$  ppm, that overlap with the resonances ascribed to the interaction with Brønsted sites and are, thus, difficult to be discriminated in between. However, TMPO interacts more strongly with these Al-Lewis sites than with Brønsted acid sites, suggesting that these sites are populated first.

## Experimental Section

### Synthesis of nano- and micronized ZSM-5 zeolites

Tetraethyl orthosilicate (TEOS, 6.25 g) was added to a solution of water (13.48 g for nano- and 49.70 g for micronized) and tetrapropylammonium hydroxide (TPAOH, 25 wt% in water, 6.00 g) and the resulting mixture hydrolyzed at 353 K for 24 h. Thereafter, the solution containing water (2.0 g), Al(NO<sub>3</sub>)<sub>3</sub>·9H<sub>2</sub>O (0.23 g) and NaOH (0.12 g) was added to the mixture. The syntheses molar composition was: micronized ZSM-5 zeolite - 1SiO<sub>2</sub>:0.01Al<sub>2</sub>O<sub>3</sub>:0.25TPAOH:0.05Na<sub>2</sub>O:100 H<sub>2</sub>O; nanosized ZSM-5 zeolite - 1SiO<sub>2</sub>:0.01Al<sub>2</sub>O<sub>3</sub>:0.25TPAOH:0.05Na<sub>2</sub>O:25 H<sub>2</sub>O. The as-prepared precursors were subjected to hydrothermal treatment at 443 K for 24 h (nanosized zeolite) and 463 K for 48 h (micronized zeolite). The ensuing ZSM-5 samples were collected by centrifugation and calcined in air at 823 K, to remove the organic template (TPA<sup>+</sup>).

The calcined ZSM-5 zeolites were transformed into the proton form (H-ZSM-5) as follows: calcined samples were treated twice with aqueous 1M NH<sub>4</sub>NO<sub>3</sub> at 353 K for 3 h, followed by activation at 823 K for 10 h.

### TMPO adsorption

50 mg of hydrated ZSM-5 were packed into 4 mm NMR rotors. The packed rotors were placed in a specially designed cell allowing dehydration under vacuum and closing the rotor under inert atmosphere. The samples were dehydrated at 573 K under high vacuum ( $< 10^{-5}$  mbar) overnight, transferred to an Argon-filled glove box, and 2.5 mg of TMPO were added to the dehydrated zeolite. The closed NMR rotors containing the zeolite and the TMPO were then heated at 423 K for 4 h.

### Crystal structure and particle size

The crystallinity of the materials was investigated by powder X-ray diffraction (XRD) on a PANalytical X'Pert Pro diffractometer using CuK $\alpha$  monochromatized radiation ( $\lambda = 1.5418$  Å).

The hydrodynamic diameter of the zeolite samples in water suspensions was determined with a Malvern Zetasizer Nano Dynamic Light Scattering (DLS) instrument. The analyses were performed on samples after purification with a solid concentration of 10 wt. % and pH=8. The backscattering geometry (scattering angle 173°, HeNe laser with 3 mW output power at 632.8 nm wavelength) allows measurements at high sample concentration, since a complete penetration of the incident light through the sample was not required. In addition, the particle size and surface features of the zeolite crystals were characterized by scanning electron microscopy (SEM) using a Hitachi SU-70 operating at 15 kV and 14.6 mm of working distance.

### Textural properties

Low temperature nitrogen adsorption/desorption isotherms were measured on a Micrometrics ASAP 2020 volumetric adsorption analyzer. Prior to the measurements, the samples were degassed at 523 K under vacuum for 12 h. The external surface area and micropore volume were estimated by the alpha-plot method using Silica-1000 ( $22.1 \text{ m}^2 \cdot \text{g}^{-1}$ ) as the reference. The micropore and mesopore size distributions of samples were estimated from the desorption branches of the isotherms, by the Nonlocal Density Functional Theory (NLDFT) and Barret-Joyner-Halenda (BJH) methods, respectively.

### NMR spectroscopy

$^{31}\text{P}$  and  $^1\text{H}$  NMR spectra were recorded at 161.9 and 400.1 MHz, respectively, on a 9.4 T Bruker Avance III 400 spectrometer using a 4 mm Bruker magic-angle spinning (MAS) probe. Chemical shifts are quoted in ppm from TMS using as secondary references solid adamantane ( $^1\text{H}$ , 1.85 ppm) and solid  $\text{Na}_4\text{P}_2\text{O}_7$  ( $^{31}\text{P}$ , most shielded resonance -2.09 ppm).  $^1\text{H}$ -decoupled  $^{31}\text{P}$  MAS NMR spectra were recorded with a spinning rate of 15 kHz and 3.2  $\mu\text{s}$  pulses ( $90^\circ$  flip angle) corresponding to a radiofrequency (rf) field strength of 78 kHz. A 20 s recycle delay (RD) was used.  $^1\text{H}$ - $^{31}\text{P}$  HETCOR NMR spectra were recorded with a  $^1\text{H}$  2.8  $\mu\text{s}$  pulses ( $90^\circ$  flip angle) corresponding to a rf of 90 kHz. The cross-polarization step used a contact time of 3500  $\mu\text{s}$ , with a 70–100% RAMP shape on the  $^1\text{H}$  channel and a square shaped pulse of 51 kHz on the  $^{31}\text{P}$  channel, a 2.25 s RD, and a spinning rate of 15 kHz. A SPINAL-64 decoupling scheme was used with 6  $\mu\text{s}$  pulses at a rf field strength of 80 kHz.[30] 145 t1 points with 2048 scans each were recorded in the indirect dimension. The simulation of the  $^{31}\text{P}$  NMR spectra was carried out using Gaussian/Lorentzian curves as implemented in the DMFIT software.[31]

### Computational calculations

Periodic models of the external H-ZSM-5 surface were constructed using the procedure of Treps et al.[15] Herein, we consider sites arising from the cleave along the (100) crystallographic plane present in both the rounded-boat and coffin-shaped crystals.[32] Terminal SiO bonds were saturated with hydrogen atoms to create SiOH groups. Some Si atoms were replaced by Al atoms to create bridging hydroxyl groups at the pore-mouth and Al-H<sub>2</sub>O groups at the external surface. We used the site nomenclature of Treps et al., for sake of simplicity.[15] A 25 Å vacuum layer was added on top of the cleaved surface resulting in cells with  $a = 20.00$ ,  $b = 13.36$  and  $c = 64.44$  Å, and an almost orthorhombic cell with  $\alpha$  and  $\beta = 90.00$ ,  $\gamma = 89.99^\circ$ . The internal SiOH nest was built by removing one Si atom at the channel intersection and saturating the four surrounding O atoms with H atoms in a  $1 \times 1 \times 2$  supercell of the MFI framework.

Periodic DFT calculations were performed with the PBE exchange correlation functional,[33] with Grimme's D3 dispersion correction,[34] as implemented in CP2K code version 6.1.[35,36] All periodic calculations used a plane wave energy cutoff of 800 Ry, the Goedecker–Teter–Hutter pseudopotentials devised by Krack,[37] and triple-zeta Gaussian basis sets (TZVP-MOLOPT-GTH).[38] The structures were considered fully converged when the change between consecutive optimization steps was below  $5 \times 10^{-5}$  Bohr, and the residual forces were

smaller than  $5 \times 10^{-6}$  Ha Bohr<sup>-1</sup>. The optimized structures were cleaved into large clusters containing 94 T sites, and the terminal O atoms were replaced by H atoms. These clusters were used to compute the  $^{31}\text{P}$  and  $^1\text{H}$  NMR isotropic chemical shifts using the gauge-independent atomic orbital methods, combined with the PBE0 functional,[39] and the 6-311G(2d,2p) basis sets,[40,41] as implemented in the Gaussian 16 revision C.01.[42]

### Acknowledgements

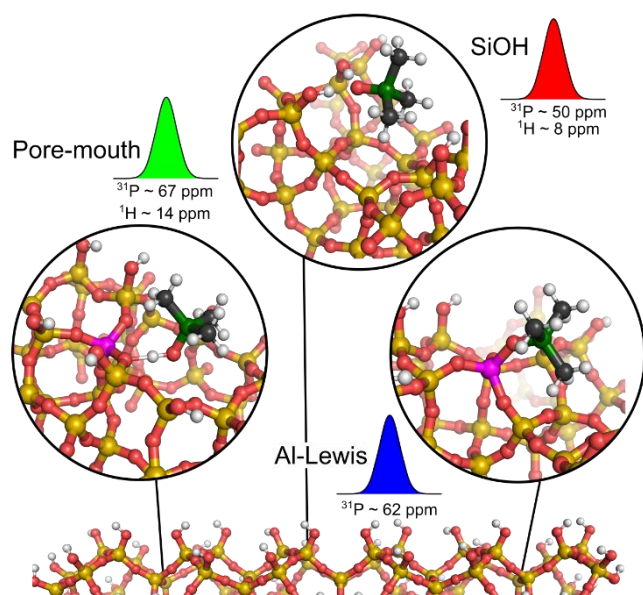
C. Bornes acknowledges FCT for Doctoral Fellowship PD/BD/142849/2018 integrated in the Ph.D. programme in NMR applied to chemistry, materials, and biosciences (Grant PD/00065/2013). This work was developed within the scope of the project CICECO-Aveiro Institute of Materials, Grants UIDB/50011/2020, UIDP/50011/2020 and LA/P/0006/2020, financed by national funds through the FCT/MEC (PIDDAC). The NMR spectrometers are part of the National NMR Network (PTNMR) and are partially supported by Infrastructure Project No. 022161 (co-financed by FEDER through COMPETE 2020, POCI and PORL and FCT through PIDDAC). Computing resources provided by STFC Scientific Computing Department's SCARF cluster. We thank Dr. Céline Chizallet for providing some models that were adapted to this work. We acknowledge the support of the Label of Excellence for the Centre for zeolites and nanoporous materials by the Region of Normandy (CLEAR). CFGCG thanks the FCT for funding the Coimbra Chemistry Centre through the programmes UIDB/00313/2020 and UIDP/00313/2020, also co-funded by FEDER/COMPETE 2020-EU.

**Keywords:** nanozeolites • external surface • acidity • solid-state NMR • hydroxyls

- [1] M.E. Davis, Zeolite-based catalysts for chemicals synthesis, *Microporous and Mesoporous Materials*, 21 (1998) 173–182. [https://doi.org/10.1016/S1387-1811\(98\)00007-9](https://doi.org/10.1016/S1387-1811(98)00007-9).
- [2] D. Xu, G.R. Swindlehurst, H. Wu, D.H. Olson, X. Zhang, M. Tsapatsis, Zeolites: On the Synthesis and Adsorption Properties of Single-Unit-Cell Hierarchical Zeolites Made by Rotational Intergrowths (*Adv. Funct. Mater.* 2/2014), *Advanced Functional Materials*, 24 (2014) 200–200. <https://doi.org/10.1002/adfm.201470011>.
- [3] S. Kesraoui-Ouki, C.R. Cheeseman, R. Perry, Natural zeolite utilisation in pollution control: A review of applications to metals' effluents, *Journal of Chemical Technology & Biotechnology*, 59 (1994) 121–126. <https://doi.org/10.1002/jctb.280590202>.
- [4] K. Tanabe, W.F. Hölderich, Industrial application of solid acid–base catalysts, *Applied Catalysis A: General*, 181 (1999) 399–434. [https://doi.org/10.1016/S0926-860X\(98\)00397-4](https://doi.org/10.1016/S0926-860X(98)00397-4).
- [5] H. Chen, Y. Wang, F. Meng, H. Li, S. Wang, C. Sun, S. Wang, X. Wang, Conversion of methanol to propylene over nano-sized ZSM-5 zeolite aggregates synthesized by a modified seed-induced method with CTAB, *RSC Adv.* 6 (2016) 76642–76651. <https://doi.org/10.1039/C6RA14753D>.
- [6] Z. Yan, D. Ma, J. Zhuang, X. Liu, X. Liu, X. Han, X. Bao, In situ solid state NMR observation of the methanol-to-hydrocarbons (MTH) process over nanosized and microsized HZSM-5 zeolites, *Phys. Chem. Chem. Phys.* 4 (2002) 4602–4607. <https://doi.org/10.1039/B201897G>.
- [7] L. Yang, Z. Liu, Z. Liu, W. Peng, Y. Liu, C. Liu, Product distribution and catalytic performance of nano-sized H-ZSM-5 zeolites in the methanol-to-aromatics (MTA) reaction, *Petroleum Science and Technology*, 35 (2017) 955–962. <https://doi.org/10.1080/10916466.2017.1292293>.
- [8] K. Rajagopalan, A.W. Peters, G.C. Edwards, Influence of zeolite particle size on selectivity during fluid catalytic cracking, *Applied Catalysis*, 23 (1986) 69–80. [https://doi.org/10.1016/S0166-9834\(00\)81453-0](https://doi.org/10.1016/S0166-9834(00)81453-0).
- [9] A.J.H.P. van der Pol, A.J. Verduyn, J.H.C. van Hooff, Why are some titanium silicalite-1 samples active and others not?, *Applied Catalysis A: General*, 92 (1992) 113–130. [https://doi.org/10.1016/0926-860X\(92\)80310-9](https://doi.org/10.1016/0926-860X(92)80310-9).

- [10] K. Beschmann, L. Riekert, Isomerization of Xylene and Methylation of Toluene on Zeolite H-ZSM-5. Compound Kinetics and Selectivity, *Journal of Catalysis*. 141 (1993) 548–565. <https://doi.org/10.1006/jcat.1993.1163>.
- [11] C. Herrmann, J. Haas, F. Fetting, Effect of the crystal size on the activity of ZSM-5 catalysts in various reactions, *Applied Catalysis*. 35 (1987) 299–310. [https://doi.org/10.1016/S0166-9834\(00\)82868-7](https://doi.org/10.1016/S0166-9834(00)82868-7).
- [12] W. Zhang, X. Bao, X. Guo, X. Wang, A high-resolution solid-state NMR study on nano-structured HZSM-5 zeolite, *Catalysis Letters*. 60 (1999) 89–94. <https://doi.org/10.1023/A:1019061714047>.
- [13] B. Louis, A. Vicente, C. Fernandez, V. Valtchev, Crystal Size–Acid Sites Relationship Study of Nano- and Micrometer-Sized Zeolite Crystals, *J. Phys. Chem. C*. 115 (2011) 18603–18610. <https://doi.org/10.1021/jp204234d>.
- [14] B. Gehring, Y. Traa, M. Hunger, Elucidation of the versatile brønsted acidity of nanosized ZSM-5 materials, *Microporous and Mesoporous Materials*. (2021) 110978. <https://doi.org/10.1016/j.micromeso.2021.110978>.
- [15] L. Treps, A. Gomez, T.D. Bruin, C. Chizzallet, Environment, Stability and Acidity of External Surface Sites of Silicalite-1 and ZSM-5 Micro and Nano Slabs, Sheets, and Crystals, *ACS Catalysis*. 10 (2020) 3297–3312. <https://doi.org/10.1021/acscatal.9b05103>.
- [16] J.H. Koegler, H. van Bekkum, J.C. Jansen, Growth model of oriented crystals of zeolite Si-ZSM-5, *Zeolites*. 19 (1997) 262–269. [https://doi.org/10.1016/S0144-2449\(97\)00088-2](https://doi.org/10.1016/S0144-2449(97)00088-2).
- [17] M.B.J. Roelfaers, R. Ameloot, M. Baruah, H. Uji-i, M. Bulut, G. De Cremer, U. Müller, P.A. Jacobs, J. Hofkens, B.F. Sels, D.E. De Vos, Morphology of Large ZSM-5 Crystals Unraveled by Fluorescence Microscopy, *J. Am. Chem. Soc.* 130 (2008) 5763–5772. <https://doi.org/10.1021/ja7113147>.
- [18] H. Mochizuki, T. Yokoi, H. Imai, R. Watanabe, S. Namba, J.N. Kondo, T. Tatsumi, Facile control of crystallite size of ZSM-5 catalyst for cracking of hexane, *Microporous and Mesoporous Materials*. 145 (2011) 165–171. <https://doi.org/10.1016/j.micromeso.2011.05.011>.
- [19] M. Hunger, Multinuclear solid-state NMR studies of acidic and non-acidic hydroxyl protons in zeolites, *Solid State Nuclear Magnetic Resonance*. 6 (1996) 1–29. [https://doi.org/10.1016/0926-2040\(95\)01201-X](https://doi.org/10.1016/0926-2040(95)01201-X).
- [20] C. Bornes, M. Fischer, J.A. Amelse, C.F.G.C. Geraldes, J. Rocha, L. Mafrá, What Is Being Measured with P-Bearing NMR Probe Molecules Adsorbed on Zeolites?, *J. Am. Chem. Soc.* 143 (2021) 13616–13623. <https://doi.org/10.1021/jacs.1c05014>.
- [21] F. Dubray, E. Dib, I. Medeiros-Costa, C. Aquino, D. Minoux, S.V. Daele, N. Nesterenko, J.-P. Gilson, S. Mintova, The challenge of silanol species characterization in zeolites, *Inorganic Chemistry Frontiers*. (2022). <https://doi.org/10.1039/D1QI01483H>.
- [22] C. Bornes, M. Sardo, Z. Lin, J. Amelse, A. Fernandes, M.F. Ribeiro, C. Geraldes, J. Rocha, L. Mafrá, 1H–31P HETCOR NMR elucidates the nature of acid sites in zeolite HZSM-5 probed with trimethylphosphine oxide, *Chemical Communications*. 55 (2019) 12635–12638. <https://doi.org/10.1039/C9CC06763A>.
- [23] S. Lang, M. Benz, U. Obenaus, R. Himmelmann, M. Hunger, Novel Approach for the Characterization of Lewis Acidic Solid Catalysts by Solid-State NMR Spectroscopy, *ChemCatChem*. 8 (2016) 2031–2036. <https://doi.org/10.1002/cctc.201600372>.
- [24] A. Zheng, H. Zhang, X. Lu, S.B. Liu, F. Deng, Theoretical predictions of <sup>31</sup>P NMR chemical shift threshold of trimethylphosphine oxide adsorbed on solid acid catalysts, *Journal of Physical Chemistry B*. 112 (2008) 4496–4505. <https://doi.org/10.1021/jp709739v>.
- [25] G. Engelhardt, B. Fahlke, M. Mägi, E. Lippmaa, High-Resolution <sup>29</sup>Si and <sup>27</sup>Al NMR Studies of <sup>29</sup>Si-enriched ZSM-5 Zeolites, *Zeitschrift Für Physikalische Chemie*. 2660 (1985) 239–245. <https://doi.org/10.1515/zpch-1985-26636>.
- [26] Y. Wang, S. Xin, Y. Chu, J. Xu, G. Qi, Q. Wang, Q. Xia, F. Deng, Influence of Trimethylphosphine Oxide Loading on the Measurement of Zeolite Acidity by Solid-State NMR Spectroscopy, *J. Phys. Chem. C*. 125 (2021) 9497–9506. <https://doi.org/10.1021/acs.jpcc.1c01789>.
- [27] M. Wang, Y. Han, S. Liu, Z. Liu, D. An, Z. Zhang, K. Cheng, Q. Zhang, Y. Wang, Pore-mouth catalysis boosting the formation of iso-paraffins from syngas over bifunctional catalysts, *Chinese Journal of Catalysis*. 42 (2021) 2197–2205. [https://doi.org/10.1016/S1872-2067\(20\)63770-6](https://doi.org/10.1016/S1872-2067(20)63770-6).
- [28] J.A. Martens, G. Vanbutsele, P.A. Jacobs, J. Denayer, R. Ocakoglu, G. Baron, J.A. Muñoz Arroyo, J. Thybaut, G.B. Marin, Evidences for pore mouth and key–lock catalysis in hydroisomerization of long n-alkanes over 10-ring tubular pore bifunctional zeolites, *Catalysis Today*. 65 (2001) 111–116. [https://doi.org/10.1016/S0920-5861\(00\)00577-0](https://doi.org/10.1016/S0920-5861(00)00577-0).
- [29] I.C. Medeiros-Costa, E. Dib, N. Nesterenko, J.-P. Dath, J.-P. Gilson, S. Mintova, Silanol defect engineering and healing in zeolites: opportunities to fine-tune their properties and performances, *Chem. Soc. Rev.* 50 (2021) 11156–11179. <https://doi.org/10.1039/D1CS00395J>.
- [30] B.M. Fung, A.K. Khitrin, K. Ermolaev, An Improved Broadband Decoupling Sequence for Liquid Crystals and Solids, *Journal of Magnetic Resonance*. 142 (2000) 97–101. <https://doi.org/10.1006/jmre.1999.1896>.
- [31] D. Massiot, F. Fayon, M. Capron, I. King, S. Le Calvé, B. Alonzo, J.O. Durand, B. Bujoli, Z. Gan, G. Hoatson, Modelling one- and two-dimensional solid-state NMR spectra, *Magnetic Resonance in Chemistry*. 40 (2002) 70–76. <https://doi.org/10.1002/mrc.984>.
- [32] G. Zeng, C. Chen, D. Li, B. Hou, Y. Sun, Exposure of (001) planes and (011) planes in MFI zeolite, *CrystEngComm*. 15 (2013) 3521. <https://doi.org/10.1039/c3ce40142a>.
- [33] J.P. Perdew, K. Burke, M. Ernzerhof, Generalized Gradient Approximation Made Simple, *Phys. Rev. Lett.* 77 (1996) 3865–3868. <https://doi.org/10.1103/PhysRevLett.77.3865>.
- [34] S. Grimme, J. Antony, S. Ehrlich, H. Krieg, A consistent and accurate *ab initio* parametrization of density functional dispersion correction (DFT-D) for the 94 elements H–Pu, *The Journal of Chemical Physics*. 132 (2010) 154104. <https://doi.org/10.1063/1.3382344>.
- [35] J. VandeVondele, M. Krack, F. Mohamed, M. Parrinello, T. Chassaing, J. Hutter, Quickstep: Fast and accurate density functional calculations using a mixed Gaussian and plane waves approach, *Computer Physics Communications*. 167 (2005) 103–128. <https://doi.org/10.1016/j.cpc.2004.12.014>.
- [36] T.D. Kühne, M. Iannuzzi, M. Del Ben, V.V. Rybkin, P. Seewald, F. Stein, T. Laino, R.Z. Khaliullin, O. Schütt, F. Schiffmann, D. Golze, J. Wilhelm, S. Chulkov, M.H. Bani-Hashemian, V. Weber, U. Borstnik, M. Taillefumier, A.S. Jakobovits, A. Lazzaro, H. Pabst, T. Müller, R. Schade, M. Guidon, S. Andermatt, N. Holmberg, G.K. Schenter, A. Hehn, A. Bussy, F. Belleflamme, G. Tabacchi, A. GlöB, M. Lass, I. Bethune, C.J. Mundy, C. Plessl, M. Watkins, J. VandeVondele, M. Krack, J. Hutter, CP2K: An Electronic Structure and Molecular Dynamics Software Package -- Quickstep: Efficient and Accurate Electronic Structure Calculations, (2020) 1–52. <https://doi.org/10.1007/s00214-005-0655-y>.
- [37] M. Krack, Pseudopotentials for H to Kr optimized for gradient-corrected exchange–correlation functionals, *Theor Chem Acc*. 114 (2005) 145–152. <https://doi.org/10.1007/s00214-005-0655-y>.
- [38] J. VandeVondele, J. Hutter, Gaussian basis sets for accurate calculations on molecular systems in gas and condensed phases, *The Journal of Chemical Physics*. 127 (2007) 114105. <https://doi.org/10.1063/1.2770708>.
- [39] C. Adamo, V. Barone, Toward reliable density functional methods without adjustable parameters: The PBE0 model, *J. Chem. Phys.* 110 (1999) 6158–6170. <https://doi.org/10.1063/1.478522>.
- [40] A.D. McLean, G.S. Chandler, Contracted Gaussian basis sets for molecular calculations. I. Second row atoms, Z=11–18, *J. Chem. Phys.* 72 (1980) 5639–5648. <https://doi.org/10.1063/1.438980>.
- [41] R. Krishnan, J.S. Binkley, R. Seeger, J.A. Pople, Self-consistent molecular orbital methods. XX. A basis set for correlated wave functions, *J. Chem. Phys.* 72 (1980) 650–654. <https://doi.org/10.1063/1.438955>.
- [42] M.J. Frisch, G.W. Trucks, H.B. Schlegel, G.E. Scuseria, M.A. Robb, J.R. Cheeseman, G. Scalmani, V. Barone, G.A. Petersson, H. Nakatsuji, X. Li, M. Caricato, A.V. Marenich, J. Bloino, B.G. Janesko, R. Gomperts, B. Mennucci, H.P. Hratchian, J.V. Ortiz, A.F. Izmaylov, J.L. Sonnenberg, Williams, F. Ding, F. Lipparini, F. Egidi, J. Goings, B. Peng, A. Petrone, T. Henderson, D. Ranasinghe, V.G. Zakrzewski, J. Gao, N. Rega, G. Zheng, W. Liang, M. Hada, M. Ehara, K. Toyota, R. Fukuda, J. Hasegawa, M. Ishida, T. Nakajima, Y. Honda, O. Kitao, H. Nakai, T. Vreven, K. Throssell, J.A. Montgomery Jr., J.E. Peralta, F. Ogliaro, M.J. Bearpark, J.J. Heyd, E.N. Brothers, K.N. Kudin, V.N. Staroverov, T.A. Keith, R. Kobayashi, J. Normand, K. Raghavachari, A.P. Rendell, J.C. Burant, S.S. Iyengar, J. Tomasi, M. Cossi, J.M. Millam, M. Klene, C. Adamo, R. Cammi, J.W. Ochterski, R.L. Martin, K. Morokuma, O. Farkas, J.B. Foresman, D.J. Fox, *Gaussian 16 Rev. C.01*, Wallingford, CT, 2016.

Entry for the Table of Contents



The structure and acid properties of external sites of ZSM-5 zeolites, namely terminal SiOH groups, pore-mouth Brønsted, and tricoordinated Al-Lewis acid sites, are elucidated via the interaction of samples of distinct particle size with the NMR probe molecule trimethylphosphine oxide, assisted by computational methods.

Institute and/or researcher Twitter usernames: teamspecko, ciceco\_ua, labo\_lcs, carlospornes, smintova, joaroc50726897, luis\_mafra007